ELSEVIER

Journal of Alloys and Compounds 228 (1995) 181–187

Journal of ALLOYS AND COMPOUNDS

Crystal structure and phase composition of alloys $Zr_{1-x}Ti_x(Mn_{1-y}V_y)_2$

J. Huot[a], E. Akiba[a], H. Iba[b]

[a]*National Institute of Materials and Chemical Research, 1-1 Higashi, Tsukuba, Ibaraki 305, Japan*
[b]*Material Engineering Division 1, Toyota Motor Corporation, 1, Toyota-cho, Toyota, Aichi 471, Japan*

Received 31 January 1995; in final form 3 May 1995

Abstract

The crystal structure and morphology of the Laves-phase alloys $Zr_{1-x}Ti_x(Mn_{1-y}V_y)_2$, have been studied by X-ray powder diffraction and transmission electron microscopy (TEM). Hydriding properties were analyzed from pressure–composition (PC) isotherms. Most of the alloys were multiphase, with up to four phases simultaneously present in one alloy. The identified phases were: hexagonal C14 and cubic C15 Laves phases, bcc solid solution, α-ZrO_2 and η-carbide-type oxide. A qualitative phase map of the system was constructed. TEM measurements indicated that the Laves phase C14 and the bcc solid solution have preferential atomic composition. To clarify this result, the alloys $Zr_{0.6}Ti_{0.4}Mn_{1.1}V_{0.9}$ and $Ti_{0.2}Mn_{0.2}V_{0.6}$ were prepared and analyzed by X-ray powder diffraction. The hydrogen capacity on the system $Zr_{1-x}Ti_xMnV$ by PC measurements agreed with the value calculated by the capacity and abundance of each end member phase.

Keywords: Crystal structure; Hydrogen absorption; Phase composition

1. Introduction

Because of their potentially high hydrogen absorption capacity, Laves-phase AB_2-type alloys are now actively studied. Potential applications are hydrogen storage, heat transportation, hydrogen getters and electrode for rechargeable battery [1–3].

Laves phases are typified by three prototype structures based on magnesium: $MgZn_2$ (hexagonal C14), $MgCu_2$ (cubic C15) and $MgNi_2$ (hexagonal C36). These structures are described by different stacking of layers of atoms [4]. Geometrical factors play an important role in determining the stability of these phases [5,6]. Electron concentration also contributes to the relative stability of the different phases. The C14 and C15 structures are the most frequently encountered and also the most interesting for technological applications.

In an earlier study on the systems (Zr, A)$V_{0.5}Ni_{1.1}Mn_{0.2}Fe_{0.2}$ where A = Ti, Nb and Hf [7], it was found that most of the alloys of these systems were multiphases. In particular, the multiphase alloy $Zr_{0.75}Ti_{0.25}V_{0.5}Ni_{1.1}Mn_{0.2}Fe_{0.2}$ was formed by a bcc and a C14 phase. From pressure–composition (PC) measurements, it was shown that this alloy behaves as a single phase. Therefore, this bcc phase is called the "Laves-phase-related bcc phase". The conditions of disappearance of a particular phase were also investigated.

In this work, we further investigated the nature of multiphase alloys by examining the much simpler system $Zr_{1-x}Ti_x(Mn_{1-y}V_y)_2$. The four end-members of this system have different crystal structures and are typical alloys of the AB_2-type formula. The structure of $ZrMn_2$ and $TiMn_2$, ZrV_2, and TiV_2 is C14, C15, and bcc solid solution, respectively. By substitution on A and B sites of end-members, multiphase alloys are likely to be produced. Therefore, a systematic study of this system can give important information about the condition of appearance of a particular phase and about the phase abundance in a multiphase alloy. The nature of individual phases was also investigated. In the multiphase alloys $Zr_{1-x}Ti_xMnV$ the relation between phase abundance and hydrogen capacity was studied.

The system $Zr_{1-x}Ti_x(Mn_{1-y}V_y)_2$ was investigated by X-ray powder diffraction, transmission electron microscopy (TEM), microprobe analysis (EDX) and PC isotherms. It has been described elsewhere how the Rietveld method can be effectively used for phase identification and phase abundance in multiphase alloys [8]. However, phase composition could not be

SSDI 0925-8388(95)01884-0

determined because it is impossible to distinguish between constituent atoms by X-ray powder diffraction. On the other hand, TEM and EDX measurements can give accurate atomic composition of a narrow area. Therefore, the combination of Rietveld refinement of X-ray powder diffraction and TEM–EDX measurements is a powerful tool for a complete investigation of phase composition in a multiphase alloy.

2. Experimental details

For a complete investigation of the $Zr_{1-x}Ti_x(Mn_{1-y}V_y)_2$ system, 13 alloys of different compositions were prepared. These alloys are presented in a matrix form in Fig. 1. The filled triangles indicate the alloy compositions that were prepared and investigated in this work. The alloys were made by arc-melting the raw metals (minimum purity 99.9%) in a water-cooled copper crucible under an argon atmosphere. The alloys were turned over four times during preparation to insure homogeneity. All alloys were measured without further heat treatment.

A Rigaku diffractometer with a Cu Kα radiation was used for powder X-ray diffraction measurements. The diffraction patterns were analyzed by the Rietveld method, using RIETAN software [9]. Because most of the alloys were multiphase, a procedure using Rietveld refinement was devised for phase identification. The procedure is described in detail elsewhere [8]. In the C14 phase, zirconium and titanium were assumed to be randomly distributed on the A site, while the vanadium and manganese atoms were randomly distributed on the B site. For the bcc phase there is one site to be occupied by a metal atom, therefore all atoms were assumed to be randomly distributed on this site.

The TEM measurements were taken on a JEOL JEM-2000FX apparatus. The PC isotherms were measured at 200°C by a conventional constant volume apparatus [10]. Before PC isotherm measurements, the alloys were pretreated by evacuating at 400°C for 2 h.

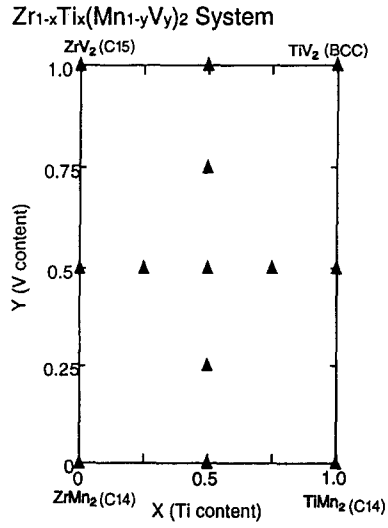

Fig. 1. Matrix of the system $Zr_{1-x}Ti_xMn_{1-y}V_y$. Triangles indicate the alloys prepared and analyzed in this work.

3. Results and discussion

3.1. Phase abundance and crystal structure

For all alloys, the Rietveld refinement method of the X-ray powder diffraction pattern was used to determine the nature and abundance of constituent phases. The powder diffraction pattern of the as-cast alloy $Zr_{0.75}Ti_{0.25}MnV$ is shown in Fig. 2 as a representative measurement. The experimental points are indicated by dots, while the upper curve is the calculated profile by the Rietveld refinement. The position of Bragg's reflections of two phases are indicated by small bars. The lower curve is the difference between observed and calculated intensities. This curve indicates a good fit and the absence of any other phase.

In Rietveld refinement, a variety of R values are used to ascertain the quality of the fit [11,12]. Another reliable indicator is the "goodness of the fit", defined as: $S = R_{wp}/R_e$ [11], where R_{wp} is a measure of the weighted difference between calculated and measured intensities, and R_e is an estimation of the minimum possible value of R_{wp}.

The refined parameters for the alloy $Zr_{0.75}Ti_{0.25}MnV$ are presented in Table 1. The R_{wp} and S values are 11.79% and 1.32, respectively, indicating a satisfactory global fit. Also, the R-Bragg factors (R_B)

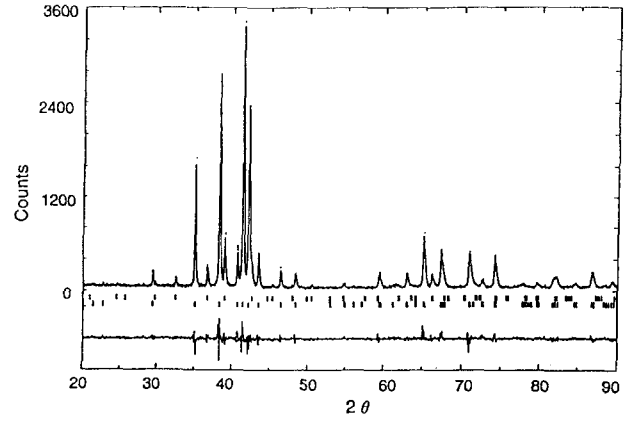

Fig. 2. X-ray powder diffraction pattern fitting by Rietveld refinement of $Zr_{0.75}Ti_{0.25}MnV$. Short vertical bars indicate the centers of Bragg reflections: upper row is η-carbide-type $\{(Zr_{0.75}Ti_{0.25})_3(MnV)_3O\}$, bottom row is C14 phase.

Table 1
Crystal structure refinement results for $Zr_{0.75}Ti_{0.25}MnV$. M1 = $Zr_{0.57}Ti_{0.43}$, M2 = $Mn_{0.54}V_{0.46}$, M3 = $Ti_{0.2}Mn_{0.2}V_{0.6}$, A = $Zr_{0.75}Ti_{0.25}$, B = $Mn_{0.5}V_{0.5}$. The value in parentheses are one standard deviation and refer to the last digit. The space group sequence number is in parentheses. Fitting parameters: R_{wp} = 11.79%; S = 1.32

Phase	Space group	R_B(%)	Lattice parameters (Å)	Atom	Wyckoff symbol	Refined coordinates	Thermal parameter
C14	$P6_3/mmc$ (194)	2.67	a = 5.1058(2) c = 8.2955(3)	M1	4f	z = 0.0608(6)	0.1
				M2	2a		1.9(3)
				M2	6h	x = 0.8314(9)	1.7(2)
A_3B_3O	$Fd3m$ (227)	5.91	a = 11.9664(6)	A	48f	x = 0.194(2)	0.349
				B	32e	$x = y = z$ = 0.830(2)	1(1)
				B	16d		3(2)
				O	16c		0.1
bcc	$Im3m$ (229)	1.9	a = 3.0066(6)	M3			0.1

are less than 6% for all three phases, indicating a good fit of crystal structure parameters [13].

In multiphase alloys, the weight fraction (W_i) of the ith phase was calculated using the relation given by Hill and Howard [14]. It should be pointed out that, when R_{wp} is larger than 15%, because of the possibility of the presence of unknown phases, the phase abundance has to be seen as an estimation, indicating mainly the relative abundance of the identified phases.

The phase abundance and R values for all alloys are shown in Table 2. Most of the alloys are multiphase, with up to four phases simultaneously present in one alloy. With the exception of the alloys $Zr_{0.5}Ti_{0.5}V_2$ and TiV_2, for all alloys the S values are lower than 2.5. For the alloy $Zr_{0.5}Ti_{0.5}V_2$, after fitting with the bcc phase, there remains a strong peak at d = 2.7104 Å. In the case of TiV_2, only the bcc phase is present, but the relative intensity of the (200) diffraction peak is too small. The η-carbide type oxide A_3B_3O is present in all alloys containing zirconium and vanadium simultaneously, with the exception of $Zr_{0.5}Ti_{0.5}Mn_{1.5}V_{0.5}$ and $Zr_{0.5}Ti_{0.5}V_2$. This oxide phase is discussed in detail elsewhere [8].

To assess fully the quality of a refined structure, other criteria than R values should be used [15]. For example, bond distances and angles should be inspected. Because of the large number of alloys investigated in this work, we limit our discussion to the bond distance in the C14 and bcc phases. Bond distances for these two phases are reported in Table 3. For C14 phase, three bond distances are reported; between the A atom on the 4f site (Wickoff notation) and the B atom on the 6h site, between two B atoms on the 6h site and between two A atoms on the 4f site. These distances were selected because the coordinates of the 4f site and 6h site have to be refined.

$ZrMn_2$ is a representative alloy of the C14 phase. Bond distances obtained in this work for $ZrMn_2$ agreed with the results of the previous work [16], therefore we regarded the results of Rietvelt refinement here as reasonable.

Table 2
R values and phase abundance obtained from the Rietveld refinement method. $S = R_{wp}/R_e$

Alloy	R_{wp} (%)	S	Phase	Phase (wt.%)	R_B (%)
$ZrMn_2$	19.13	2.41	C14	92.8(4)	10.91
			A_3B_3O	7.2(2)	13.82
ZrMnV	18.81	2.08	C14	72(3)	8.73
			A_3B_3O	15(2)	10.3
			C15	13(2)	9.86
ZrV_2	10.18	1.2	C15	37.7(3)	1.44
			A_3B_3O	25.4(2)	3.34
			V	23.5(2)	1.29
			α-Zr	13.3(2)	2.39
$Zr_{0.75}Ti_{0.25}MnV$	11.79	1.32	C14	85.2(6)	3.01
			A_3B_3O	10.0(2)	4.89
			BCC	4.8(5)	1.86
$Zr_{0.5}Ti_{0.5}Mn_2$	20.38	2.49	C14	100	5.04
$Zr_{0.5}Ti_{0.5}Mn_{1.5}V_{0.5}$	16.51	1.43	C14	100	5.98
$Zr_{0.5}Ti_{0.5}MnV$	11.81	1.22	C14	75.4(8)	2.99
			BCC	15.6(4)	2.43
			A_3B_3O	9.0(4)	2.43
$Zr_{0.5}Ti_{0.5}Mn_{0.5}V_{1.5}$	13.2	1.42	BCC	37(1)	0.61
			C14	27(3)	2.52
			A_3B_3O	18(1)	7.38
			C15	17(2)	5.32
$Zr_{0.5}Ti_{0.5}V_2$	39.53	3.36	BCC	100	21.26
$Zr_{0.25}Ti_{0.75}MnV$	14.47	1.31	C14	63.8(3)	7.15
			BCC	30.4(3)	2.3
			A_3B_3O	5.8(4)	3.32
$TiMn_2$	23.86	1.77	C14	100	8.48
TiMnV	27.21	1.65	BCC	78(1)	10.62
			C14	22(5)	13.44
TiV_2	44.06	3.81	BCC	100	45.48

In the bcc phase, we assumed that all atoms were randomly distributed on the same site. However, in the series $Zr_{1-x}Ti_xMnV$, when the zirconium atom (Goldschmidt radius, 1.60 Å) is replaced by the titanium (Goldschmidt radius, 1.47 Å), the bond distance does not change significantly. This phenomenon indicates that substitution of Ti to Zr does not play a significant role in formation of the bcc phase. Because it is hard to distinguish among Ti, Mn and V by X-ray powder diffraction, the nature of each individual phase

Table 3
Bond distances in C14 phase between the A atom in the *4f* site and the B atom in the *6h* site

Alloy	C14			bcc (Å)
	A–B (Å)	A–A (Å)	B–B (Å)	
$ZrMn_2$	2.9548	3.0821	2.4717	–
ZrMnV	2.9718	3.1342	2.4998	–
$Zr_{0.75}Ti_{0.25}MnV$	2.9616	3.1164	2.5239	2.6038
$Zr_{0.5}Ti_{0.5}Mn_2$	2.8976	3.0307	2.4772	–
$Zr_{0.5}Ti_{0.5}Mn_{1.5}V_{0.5}$	2.9159	3.0239	2.4206	–
$Zr_{0.5}Ti_{0.5}MnV$	2.9529	3.0747	2.4791	2.6235
$Zr_{0.5}Ti_{0.5}Mn_{0.5}V_{1.5}$	3.004	3.1111	2.5038	2.6577
$Zr_{0.5}Ti_{0.5}V_2$	–			2.6617
$Zr_{0.25}Ti_{0.75}MnV$	2.9246	3.0171	2.438	2.6285
$TiMn_2$	2.8145	2.8974	2.358	–
TiMnV	2.8412	2.8305	2.1024	2.6183
TiV_2	–			2.7027

should be probed by other means. This is discussed in the next section.

3.2. Phase composition

All alloys investigated in the system $Zr_{1-x}Ti_xMnV$ were multiphase. In Fig. 3 we present the C14 phase abundance in this system. The phase abundance of the C14 phase was nearly constant for $x < 0.5$ and decreased rapidly with x for $x > 0.5$. More information is obtained by investigating the bond distances. Fig. 4 shows the bond distance A–B as a function of x. Except for $x = 0$, the bond distance graph is a mirror image of the phase abundance. In particular, the fact that the bond distance changes only slightly from $x = 0$ to $x = 0.5$ indicates that substitution of Ti to Zr does not influence the nature of the C14 phase. To clarify this result, the alloys $Zr_{0.75}Ti_{0.25}MnV$ and $Zr_{0.5}Ti_{0.5}MnV$ have been investigated by TEM.

The TEM micrograph of the alloy $Zr_{0.5}Ti_{0.5}MnV$ is shown in Fig. 5. The clear area A is the most abundant phase of this sample. From S.A.D.P. measurement it was identified as the C14 phase (Fig. 5(c)). The dark

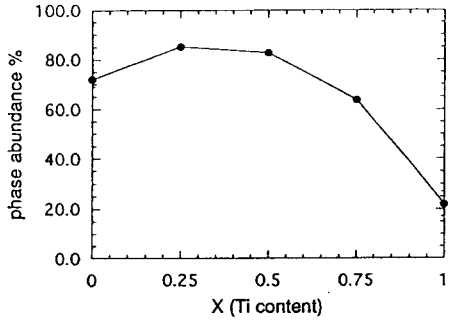

Fig. 3. C14 phase abundance by weight in the system $Zr_{1-x}Ti_xMnV$.

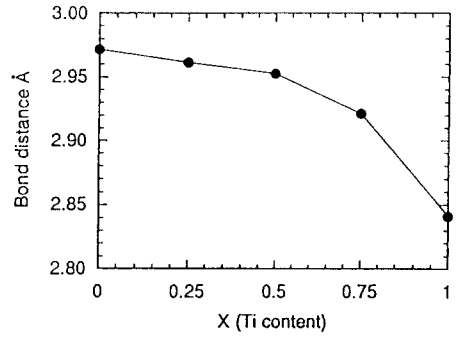

Fig. 4. Bond distances in the C14 phase between the A atom in the *4f* site and the B atom in the *6h* site in the system $Zr_{1-x}Ti_xMnV$.

colonies B cover an area of 5 to 10% of the sample analyzed by optical micrographs. Electron diffraction measurements (Fig. 5(b)) indicate that the dark colony phase has a cubic structure. It is, therefore, identified as the bcc phase. The sample contained also two other minor phases, each phase covering a surface of only 1 or 2% of the total area scanned. By EDX and electron diffraction, one phase was identified as α-ZrO_2 [17]. The other minor phase was identified as the η-carbide-type oxide [18].

In Table 4, we present the results of TEM measurements for the alloys $Zr_{0.75}Ti_{0.25}MnV$ and $Zr_{0.5}Ti_{0.5}MnV$. The C14 phase has the same composition, $Zr_{0.6}Ti_{0.4}Mn_{1.1}V_{0.9}$, for both alloys, explaining the fact that x is independent of the nature of the C14 phase. For the bcc phase, TEM measurements showed that this phase did not contain zirconium. This is in agreement with the bond distance being independent of the content of Zr. The bcc phase also has the constant atomic composition of $Ti_{0.2}Mn_{0.2}V_{0.6}$ for both samples. The η-carbide-type oxide is found to contain titanium. Therefore, we assumed that phase has the formula $(Zr_{0.75}Ti_{0.25})_3(Mn_{0.5}V_{0.5})_3O$.

These TEM measurements indicate that in multiphase alloys each phase has a specific composition, which is different from the bulk stoichiometry of the alloy.

3.3. Alloys of end-member compositions

To verify the properties of the end-member compositions of the C14 and bcc phases, we prepared alloys having the required bulk stoichiometry, i.e. $Zr_{0.6}Ti_{0.4}Mn_{1.1}V_{0.9}$ and $Ti_{0.2}Mn_{0.2}V_{0.6}$. Both alloys were measured by X-ray powder diffraction. The R values and phase abundances by weight are presented in Table 5. The alloy $Zr_{0.6}Ti_{0.4}Mn_{1.1}V_{0.9}$ is not purely C14 phase, as expected from TEM measurement of multiphase alloys. However, the C14 phase abundance is more than 92%, with bcc and η-carbide phases present at less than several percent. From Rietveld

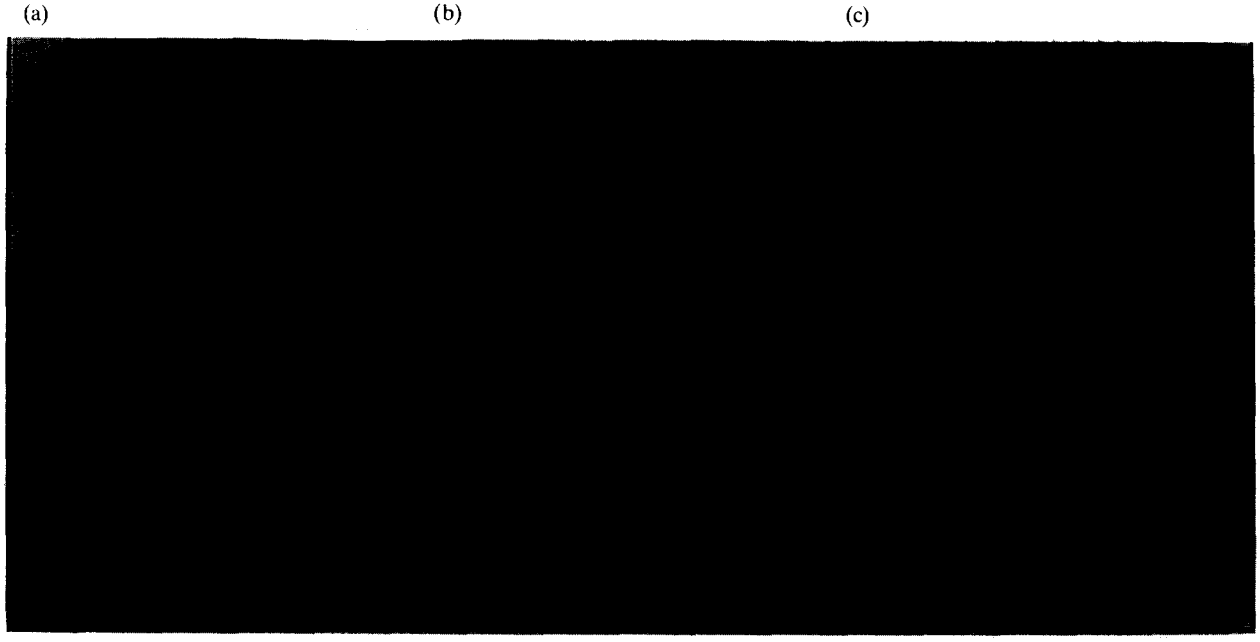

Fig. 5. TEM image of the alloy $Zr_{0.5}Ti_{0.5}MnV$: (a) bright-field image; (b) S.A.D.P. for gray area (A); (c) S.A.D.P. for matrix area (B).

Table 4
Phase composition in atomic %, measured by TEM. The values in parentheses are one standard deviation and refer to the last digit

Phase	$Zr_{0.75}Ti_{0.25}MnV$				$Zr_{0.5}Ti_{0.5}MnV$			
	Zr	Ti	Mn	V	Ar	Ti	Mn	V
C14	22(1)	12(1)	34(2)	32(1)	20(1)	15(1)	35.6(8)	29.5(1)
bcc		16(2)	18(1)	65(1)		21.7(9)	21.0(3)	57.4(7)
α-ZrO_2	100				100			
A_3B_3O	33(1)	18.7(8)	27(1)	21.4(6)				

Table 5
R values and phase abundance of the alloys $Zr_{0.6}Ti_{0.4}Mn_{1.1}V_{0.9}$ and $Ti_{0.2}Mn_{0.2}V_{0.6}$

Alloy	R_{wp} (%)	S	Phase	Phase (wt.%)	R_B (%)
$Zr_{0.6}Ti_{0.4}Mn_{1.1}V_{0.9}$	14.36	1.56	C14	92.4(4)	3.59
			bcc	6.3(7)	1.54
			A_3B_3O	1.2(1)	9.96
$Ti_{0.2}Mn_{0.2}V_{0.6}$	42.99	2.22	bcc	100	26.71

refinement, the A–B bond distance in the C14 phase was found to be 2.9421 Å. This is close to the values of bond distances in the system $Zr_{1-x}Ti_xMnV$ for $x < 0.5$.

The alloy $Ti_{0.2}Mn_{0.2}V_{0.6}$ was bcc with a very small amount of an unknown phase. We estimated the abundance of this unknown phase to be a few percent. The quite high values of R_{wp}, S and R_B are due to a bad fit of the (200) peak of the bcc phase. The experimental intensity was much larger than the calculated one. The bond distance was calculated to be 2.6191 Å. This is very close to the value of bond distances of the bcc phase in TiMnV alloys.

3.4. Phase map

From the results of TEM measurements and using the phase abundance calculated from Rietveld refinement, the phase map shown in Fig. 6 was constructed. In this map the oxide phase was omitted. Because of the limited number of experimental points, this phase map is qualitative. However, this phase map is in agreement with our measurements, and can be used for qualitative prediction on the nature and amount of each phase in the alloys of the system $Zr_{1-x}Ti_x(Mn_{1-y}V_y)_2$.

3.5. Pressure–composition isotherms

PC measurements were taken for all alloys of the system $Zr_{1-x}Ti_xMnV$. As a representative, we show in Fig. 7 the PC measurement for the alloy $Zr_{0.5}Ti_{0.5}MnV$. The curves are smooth, showing no

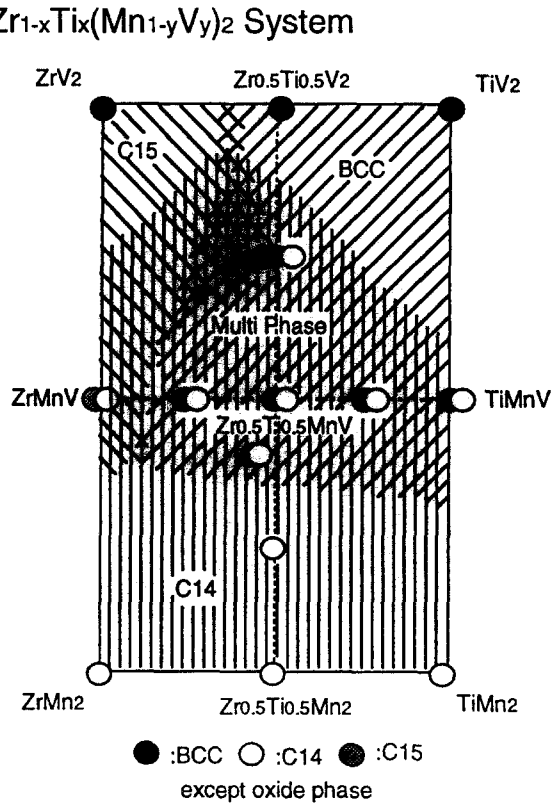

Fig. 6. Phase map of the system $(Zr_{1-x}Ti_x)(Mn_{1-y}V_y)_2$.

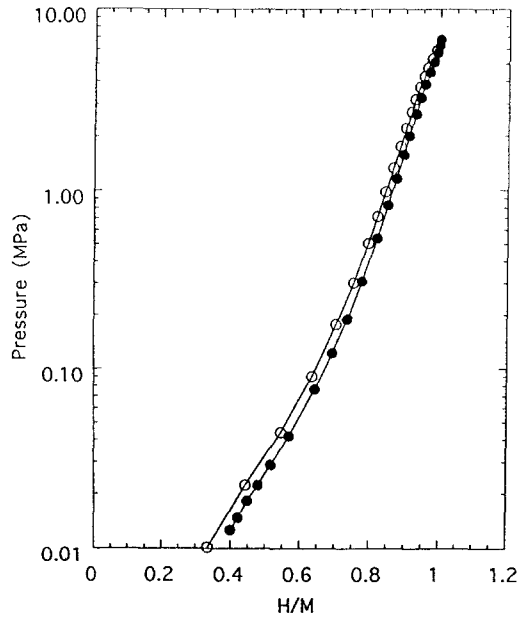

Fig. 7. Pressure–composition isotherm of $Zr_{0.5}Ti_{0.5}MnV$: ○ absorbing process; ● desorbing process.

evidence of a plateau, and with a very small hysteresis. This alloy is composed of three phases. If only one phase among three phases existing in the alloy absorbs hydrogen, that phase must have hydrogen capacity greater than H/M = 2.0. Therefore we conclude that

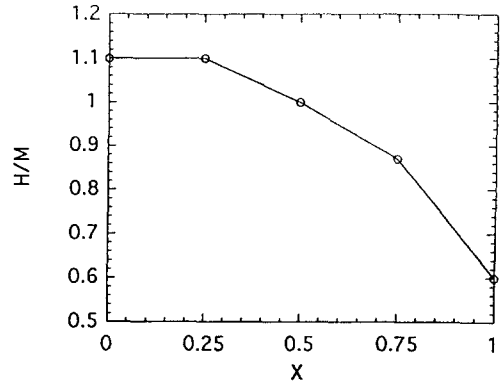

Fig. 8. Asymptotic values of PC in the system $Zr_{1-x}Ti_xMnV$.

all three phases absorb hydrogen, and that this multiphase alloy absorbs hydrogen like a single-phase alloy.

In Fig. 8, we present the asymptotic value of hydrogen/metal atom ratio (H/M) at 200°C as a function of x. This figure shows that the hydrogen capacity decreased as the abundance of the bcc phase increased.

We estimate the hydrogen capacity in the system $Zr_{1-x}Ti_xMnV$ by linear combination of the capacity and abundance of each end-member phase.

$$X_{Zr_{1-x}Ti_xMnV} = F_{bcc}X_{bcc} + F_{C14}X_{C14} + F_{C15}X_{C15} + F_{oxide}X_{oxide} \quad (1)$$

Where X is the hydrogen capacity and F the abundance of each phase. Table 6 shows the X value of each single-phase alloy. X_{C14}, X_{C15} and X_{oxide} are based on hydride structures [18–20]. X_{bcc} is the measured value of TiV_2. Because the hydrogen capacity of bcc alloy TiV_2 decreased under the experimental condition of multiphase alloys such as low activation temperature (400°C) and high PC-measurement temperature (200°C). Under these assumptions, the calculated capacity of alloys in the system $Zr_{1-x}Ti_xMnV$ (Fig. 9) agreed with measured values.

We consider that phase abundances, phase compositions and the estimation of capacity by linear combination are basic data, and a new method of design for multiphase hydrogen-absorbing alloys.

4. Conclusions

In this work, the system $Zr_{1-x}Ti_x(Mn_{1-y}V_y)_2$ was investigated by X-ray powder diffraction, TEM and pressure–composition isotherms. The Rietveld refinement of X-ray powder diffraction pattern indicated that most of the alloys are multiphase. The identified phases were the Laves phases C14 and C15, the bcc solid-solution phase and the η-carbide-type oxide. By TEM measurement it was found that the C14 and bcc

Table 6
Assumptions for estimation of hydrogen capacity

Phase	Actual composition	Assumption	Hydride structure	Ref.	H/M
C14	$Zr_{0.6}Ti_{0.4}Mn_{1.1}V_{0.9}$	$ZrMn_2$	$ZrMn_2H_{3.46}$	[19]	1.15
bcc	$Ti_{0.2}Mn_{0.2}V_{0.6}$	TiV_2	$TiV_2H_{1.8}$	–	0.60
C15	Now investigating	ZrV_2	$ZrV_2H_{4.8}$	[20]	1.60
A_3B_3O	$(Zr_{0.75}Ti_{0.25})_3(Mn_{0.5}V_{0.5})_3O$	Zr_3V_3O	$Zr_3V_3OH_{4.0}$	[18]	0.57

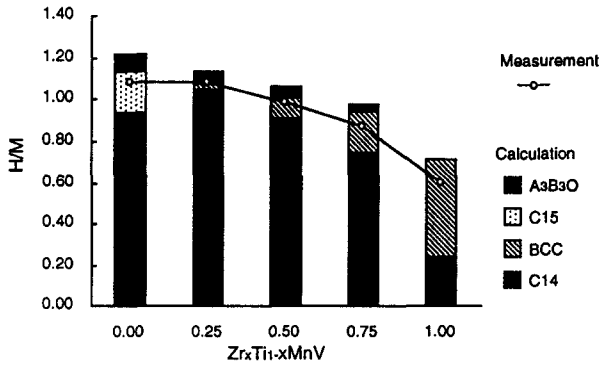

Fig. 9. Estimation of hydrogen capacity by linear combination.

phases have composition $Zr_{0.6}Ti_{0.4}Mn_{1.1}V_{0.9}$ and $Ti_{0.2}Mn_{0.2}V_{0.6}$, respectively. These compositions were assumed to be the end-member compositions of the single-phase regions. This hypothesis was verified by preparing samples with the end-member stoichiometry and analyzing them by X-ray powder diffraction. By omitting the oxide phase, a qualitative phase map was constructed. PC isotherms of the system $Zr_{1-x}Ti_xMnV$ revealed that the multiphase alloys absorbed hydrogen as a single-phase alloy. The hydrogen capacity in the system $Zr_{1-x}Ti_xMnV$ by PC measurements agreed with the value calculated by the capacity and abundance of each end-member phase.

Acknowledgments

The authors wish to thank Mr. Y. Ishido of Shin-Kobe Electric Machinery for the production of arc-melted alloys. One of the authors (J. Huot) is supported by a fellowship from the Science and Technology Agency of Japan.

References

[1] G. Sandrock, S. Suda and L. Schlapbach, in L. Schlapbach (ed.), *Hydrogen in Intermetallic Compounds II*, Springer, Berlin, 1992, Chapter 5.
[2] I. Yonezu, S. Fujitani, A. Furukawa, K. Nasalo, T. Yonesaki, T. Saito and N. Furukawa, *J. Less-Common Met., 168* (1991) 201.
[3] A. Zuttel, F. Meli and L. Schlapbach, *J. Alloys Comp., 206* (1994) 31.
[4] R. Ferro and A. Saccone, in V. Gerold (ed.), *Material Science and Technology, Vol. 1: Structure of Solids*, VCH, Weinheim, Germany, p. 182.
[5] W.B. Pearson, *Acta Cryst. B, 24* (1968) 7.
[6] W.B. Pearson, *Acta Cryst. B, 24* (1968) 1415.
[7] J. Huot, E. Akiba, T. Ogura and Y. Ishido, *J. Alloys Compounds*, in press.
[8] J. Huot, E. Akiba and Y. Ishido, *Proc. Int. Symp. on Metal–Hydrogen Systems*, Japan, 1994, to be published.
[9] F. Izumi, in R.A. Young (ed.), *The Rietveld Method*, Oxford University Press, Oxford, 1993, Chapter 13.
[10] K. Nomura, H. Uruno, S. Ono, H. Shinozuka and S. Suda, *J. Less-Common Met., 107* (1985) 221.
[11] R.A. Young, in R.A. Young (ed.), *The Rietveld Method*, Oxford University Press, Oxford, 1993, Chapter 1.
[12] R.A. Young and E. Prince, *J. Appl. Cryst., 15* (1982) 357.
[13] R.J. Hill and I.C. Madsen, *Powder Diffraction, 2* (1987) 146.
[14] R.J. Hill and C.J. Howard, *J. Appl. Cryst., 20* (1987) 467.
[15] J.E. Post and D.L. Bish, in D.L. Bish and J.E. Post (eds.), *Modern Powder Diffraction*, The Mineralogical Society of America, Washington, 1989, Chapter 9.
[16] J.-J. Didisheim, K. Yvon, D. Shaltiel and H. Shaked, *Solid State Commun., 31* (1979) 47.
[17] H. Iba and E. Akiba, *Proc. Int. Symp. on Metal–Hydrogen Systems*, Japan, 1994, to be published.
[18] J.L. Soubeyroux, L. Pontonnier, S. Miraglia, O. Isnard, D. Fruchart, E. Akiba, H. Hayakawa, S. Fujitani and I. Yonezu, *Z. Phys. Chem., 179* (1993) 187.
[19] Y. Isido, N. Nishimiya and Y. Suzuki, *Denki Kagaku, 45* (1977) 52.
[20] D. Shaltiel, I. Jacob and D. Davidov, *J. Less-Common Met., 53* (1985) 117.